Human Blood Pressure Simulation for Photoelastic Stress Analysis in Models of Vasculature

Carlos Tercero, Seiichi Ikeda, Motoki Matsushima, Toshio Fukuda
Department of Micro-Nano Systems Engineering
Nagoya University
Furo-cho 1, Chikusa-ku, Nagoya-shi 464-8603
Japan

Erick Tijerino
Mechanical, Materials and Aerospace Engineering
University of Central Florida
4000 Central Florida Blvd.
Orlando, Florida, 32816-2450
United States

Makoto Negoro
Department of Neurosurgery
Fujita Health University
1-98 Dengakugakubo, Kutsukake-cho, Toyoake, 470-1192
Japan

Ikuo Takahashi
Department of Neurosurgery
Anjo Kosei Hospital
Toukouhan No. 28 Anjo-cho, Anjo-shi, 446-8602
Japan

Abstract:
The development of a numerical criterion to evaluate the stress on models of vasculature has applications in evaluation of human skills, robots and medical tools. This criterion will enable better medical training for endovascular surgery and the development of better medical techniques and tools. We propose to use the stress produced by human blood pressure simulation in the wall of the model of vasculature as this criterion; and to measure the principal component of stress magnitude using photoelastic effect. For that we simulated human blood pressure with a 5.6% of average error, we developed a shielded urethane model of vasculature enabling water circulation and avoiding plastic deformation with pressures below 182 mmHg. We developed software to calculate the stress of the model wall. Stress produced by human blood pressure simulation and a guide wire were compared numerically in four ranges.

1. INTRODUCTION

Considering that vascular diseases are an important cause of death in human beings worldwide [1], and that the minimally invasive surgery requires the use of simulators during training of physicians to reduce costs and risk of injury during assisted interventions [2]; it is needed to develop endovascular surgery simulators. Endovascular surgery is performed by inserting a catheter from the femoral or radial artery to the section of vasculature to be treated. Through the catheter a coil can be inserted to fill in an aneurysm and avoid the blood flow to enter and prevent the rupture of the aneurysm [3], [4]. Also stents are commonly inserted through catheters to reach obstructed arteries; the blood flow is reestablished by placing a stent that expands its diameter when released from the catheter [5]. It is desirable also to develop techniques to measure performance of micro-coils and stents, and also compare the stress produced by them to the stress produced by human pressure to the wall of vasculature.

Ikeda et al. [6], proposed a method for modeling vasculature in silicone with a 13 μm accuracy enabling simulation for endovascular surgery by inserting a catheter into silicone models of vasculature from the femoral artery model to the coronary or cerebral arteries models.

Fig. 1: a) Medical training with the simulation system for endovascular surgery. b) Birefringence produced by guide wire in urethane model of aneurysm.

Even if the flow circulating trough the simulator is variable, it does not simulate human blood pressure variation, Fig. 1.a. The usage of photoelastic effect for stress visualization in models made of urethane elastomer was proposed in [7] and applied in [4] for IVR simulation, and in [8] for catheter evaluation, Fig. 1.b. By including human blood pressure in endovascular surgery simulation, we will be able to know when the catheter is applying more stress to the membrane of the model than human blood pressure. This will establish a criterion to evaluate the person or robot manipulating the catheter, and for comparing medical tools; improving the methodology proposed in [8].

J. Panza describes the human blood pressure in [9], defining a normal systolic pressure for humans as less than 120 mmHg and normal diastolic pressure less than 70 mmHg . Human coronary pressure was measured by B. De Bruyne et al. [10], having a diastolic pressure of 87.5 mmHg, and a systolic pressure of 152.5 mmHg at 1.81 Hz. Aortic pressure was measured by A. J. Ebenal et al. [11], registering a systolic pressure of 120 mmHg and a diastolic pressure of 50 mmHg at 1.3 Hz. Therefore it is required to recreate a periodically variable pressure with local minimums above 50 mmHg, and adjust the pressure variation to make a realistic reconstruction of human blood pressure wave. Homogeneous models of urethane elastomer cannot be used for that purpose as their lumen shape suffers a plastic deformation for the pressure ranges described in [9-11]; also it becomes white in contact with water.

978-1-4244-5095-4/09/$26.00 ©2009 IEEE

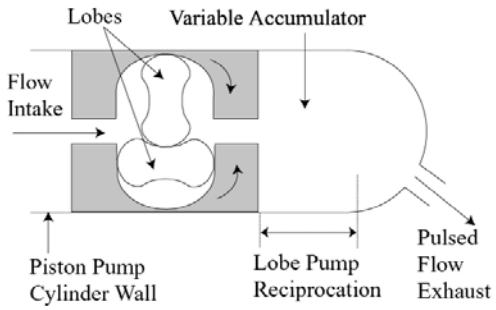

Fig.2: Schematic of the hybrid pump for human blood pressure simulation.

We propose to shield the urethane model with silicone layers to prevent plastic deformations and to isolate the urethane from environment and fluid circulation. Also we propose a hybrid pump for human blood pressure simulation that combines the properties of lobe and piston pumps and uses pressure feedback. The piston characteristics provide a carrier waveform at the heart beat frequency, and the lobe pump characteristics provide the minimum pressure and fine tuning of the waveform. We target to simulate a diastolic pressure of 57.5 mmHg, a systolic pressure of 152.5 mmHg at 1Hz, approximating the signal registered in [10], Fig.2.

2. Materials and Methods

2.1 Multilayer model of vasculature

The urethane elastomer was shielded by deep coating a wax model of vasculature fabricated using the procedure described in [6]. The first coating was done with silicone elastomer at 0.1 mm/s, the urethane elastomer coating was done 2 times at 1 mm/s after the silicone dried. After the urethane elastomer dried, silicone coating was repeated. Finally the wax was melted to complete the shielding process.

2.2 Lobe pump design

For simulating human blood pressure we need a capacity pump that provides a constant flow and an accumulator with variable volume to introduce pulsations to flow. When a piston travels along the cylinder of the pump the volume of water inside the cylinder changes; the inlet valve opens when the volume grows and the exhaust valve opens when this volume reduces. The cylinder of the piston pump has enough volume to install inside a piston shaped lobe pump. Additionally if both check valves of the piston pump are removed and the inlet sealed, we obtain a hybrid pump suitable for our simulation purposes. Lobe pumps are rotary positive displacement pumps, these pumps force fluid between two rotary elements and a static casing. The pumping flow rate is a function of lobes rotational speed, and is independent form pressure differential, Fig.2.

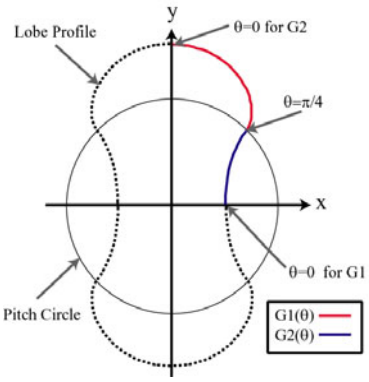

Fig. 3: Lobe profile design.

a) Lobe Profile and Mechanism

The lobe's profiles were modeled with the parametric equations following the procedure for lobe profile synthesis proposed by S. Tong el al. [12].We considered a required flow of 1 lpm, that the cross-section diameter is limited to 42 mm by the cylinder of the piston pump, and that the maximum desired speed of the motor is 400 rpm. The flow function type is sinusoidal, the flow range between 0.847 and 1.059 lpm, frequency at 3.2 kHz, a two rotor lobes configuration with a rotation speed of 800rpm.

Using the nomenclature of [12], for the above selected parameters, the corresponding non-circularity h is 0.75, the volume of the cavity V should be 2352 mm^3 and a pump with w =20 mm, obtaining the following parametric equations for the lobe profile generation that are illustrated in Fig.3:

Inner Profile:

$$G_{1x} = 6\cos(\theta) + 3\cos(2\theta)\cos(\pi - \theta) \quad (1)$$

$$G_{1y} = 6\sin(\theta) + 3\cos(2\theta)\sin(\pi - \theta) \quad (2)$$

External Profile:

$$G_{2x} = 6\cos\left(\frac{\pi}{2} - \theta\right) - 3\cos(2\theta)\cos\left(\frac{3\pi}{2} - 3\theta\right) \quad (3)$$

$$G_{2y} = 6\sin\left(\frac{\pi}{2} - \theta\right) - 3\cos(2\theta)\sin\left(\frac{3\pi}{2} - 3\theta\right) \quad (4)$$

For both equations θ varies from zero to $\pi/4$. For the first quadrant of the plane (1) and (2) define the profile inside the pitch circle and (3) and (4) define it in the outside. By symmetry the profile in the other three quadrants is generated. Figure 4 shows the hollow shaft and transmission used for coupling the reciprocating and rotational actuators to the piston shaped lobe pump, the gearbox of the lobe pump, and the lobe pump static casing.

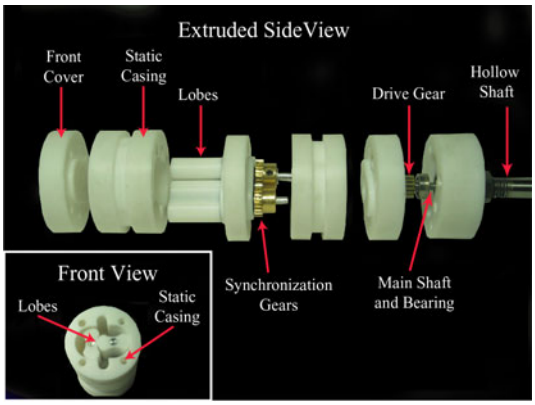

Fig.4: Mechanism inside the piston shaped lobe pump. Hollow shaft couples the lobe pump to the reciprocation and rotational motions.

b) Feedback Control

Feedback control was applied in two closed loops for controlling the reciprocation frequency and the pressure in the output of the pump, the diagram of the system is shown in figure 5. The command signal *F(z)* is a step function with the desired frequency value, and P(z) is a polynomial approximation of the human blood pressure reported in [10] . *A*, *L* and *Pi* are the transfer functions of the accumulator; lobe pump and piston pump respectively. C_1 and C_2 are P type controllers.

The function *P(z)* is periodical and synchronized to the reciprocation cycle that repeats every 2500 steps. The change of state of an optical switch marks the start of the reciprocation cycle when the volume of the accumulator reaches its minimum value. *P(z)* is defined as follows:

$$if \quad z < 1250$$

$$P(z) = -7.25\times10^{-18}z^6 + 6.59\times10^{-14}z - 2.61\times10^{-10}z^4 + 4.25\times10^{-7}z^3 - 3.1\times10^{-4}z^2 + 4.3\times10^{-2}z + 152.5 \qquad (5)$$

$$if \quad z > 1250$$

$$P(z) = -3.3\times10^{-15}z^5 + 2.6\times10^{-11}z^4 - 8.5\times10^{-8}z^3 + 1.3\times10^{-4}z^2 - 4\times10^{-2}z + 87.5 \qquad (6)$$

The system was tested to simulate human blood pressure at 1 Hz and then used to circulate flow when measuring the stress on the wall of the multilayered model of vasculature.

2.3 Image Processing Software

a) Calibration

Stress in photoelastic materials produces birefringence visible using a polariscope. Birefringence is the consequence of the phase shift between the light entering and going out of the photoelastic material [13]. That phase shift is generally called retardation, and in this paper we will name it *Re* and will be measured in nanometers.

The system shown in figure 6 was assembled and fixed for calibration and stress measurement. All analyzed and result images of this paper have 640x480 pixels, *x* and *y* are used to define the location of a pixel in a row and column of one those images. N_0 is the image of the model when filled and surrounded with water and placed between the light source and the camera. $D_{(x,y)}$ is a pixel the optical path length image N_1, and is obtained by applying equation (7) to the intensity of blue of a pixel $I_{B(x,y)}$ of N_0 [14].

$$D_{(x,y)} = -909.1 * \ln(I_{B(x,y)} / I_{B\max}) \qquad (7)$$

I_{Bmax} is the maximum value of blue in N_0, in this case equal to 255. To eliminate the noise of N_1 produced by the background all pixels with an optical path length of 0.2 mm or less where set to zero (black).We used the polariscope of [7-8] to capture images where the photoelastic effect is visible. N_2 and N_3 are images of the model of vasculature inside the polarizer, N_2 when there is no flow circulation inside the model, and N_3 when the pressure inside the model is about 182 mmHg.

Based on the results of [7, 14] we propose to model the relation between retardation $Re_{(x,y)}$ and the green intensity $I_{G(x,y)}$ in the image of urethane elastomer models as follows:

$$I_{G(x,y)} = (I_{G\max} - I_{G\min})\sin^2\frac{\pi}{\lambda_G}\mathrm{Re}_{(x,y)} + I_{G\min} \qquad (8)$$

I_{Gmin} is the minimum intensity of green between all pixels of N_2, I_{Gmax} is the maximum intensity of green between all pixels of N_3, λ_G = 538nm, is the wavelength of green light.

b) Measurement

We consider $\boldsymbol{F}$ as a collection of images obtained with the polarizer where stress should be analyzed, and F_i is one of the images of the collection and has the same number of rows, columns and pixels than N_1 ($i \in \aleph$).To calculate the retardation $Re_{(x,y)}$ in the pixel *(x, y)* of F_i; we used equation (8) with the values I_{Gmin} and I_{Gmax} obtained during the calibration, and $I_{G(x,y)}$ is the intensity of green registered at the pixel *(x, y)* of F_i.

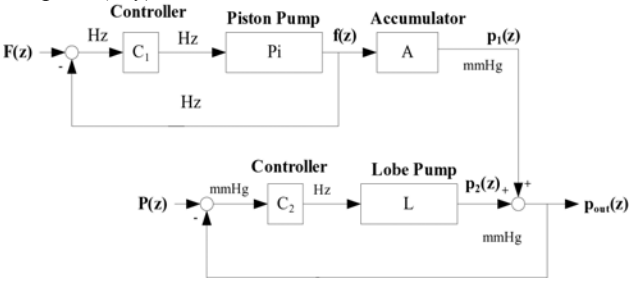

Fig.5: Control diagram of the hybrid pump.

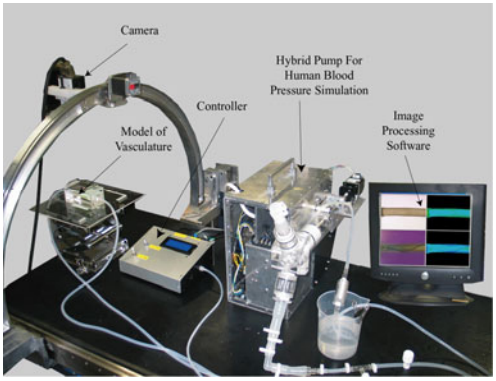

Fig.6: Experimental setup for stress quantification on the wall of the model of vasculature

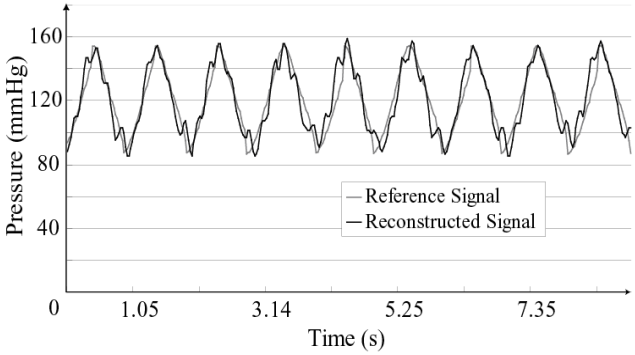

Fig.7: Human blood pressure simulation using a hybrid pump.

Then we obtain optical path length $D_{(x,y)}$ from the pixel (x, y) of N_1. Assuming the photoelastic coefficient of urethane elastomer C=3.5x10^{-9} Pa^{-1} and using equation (9) we calculate the magnitude of the principal component of stress $(\sigma_1-\sigma_2)_{(x,y)}$ in the pixel (x, y) of F_i.

$$(\sigma_1 - \sigma_2)_{(x,y)} = \frac{\mathrm{Re}_{(x,y)}}{D_{(x,y)} * C} \qquad (9)$$

The stress measurement technique was applied to eight images: N_2 for reference, $\boldsymbol{F}$ a collection of five video frames captured when hybrid pump was circulating fluid through the model (N_3= F_3), N_4, N_5 are pressure maxima of flow circulation with a guide wire applying stress to wall of the model (in N_5 the guide wire is deforming the model wall). The system integration is shown on figure 6.

3. Results

3.1 Multilayer model of vasculature

From the deep coating process we obtained a model wall with two silicone layers with a thickness of 60µm and a shielded layer of urethane elastomer with one of 250µm. Water circulation was achieved inside the model and did not suffered a plastic deformation with pressures below 182 mmHg.

3.2 Human blood pressure simulation

Human blood pressure simulation was achieved with an average error of 5.6% at a frequency of 1.01 Hz, Fig.7. When the pump was tested with model of urethane elastomer the stroke of the reciprocation was increased to raise the maximum and prove the endurance of the shielding, achieving a pressure range between 98 and 182 mmHg for registration of N_3, N_4, N_5 and $\boldsymbol{F}$. Pressure produced by the fluid was in the same ranges when the guide wire was inside and outside the model, therefore the differences in stress calculation are caused by the catheter and the model deformation.

3.3 Software Calibration

N_0 and N_1 are showed in figures 10.a and 10.b. N_1 shows an optical path length between 640 and 840 µm for the 55% of the pixels, 13.4% of the pixels of N_1 have a shorter optical path length. N_2 and N_3 are showed in figure 10.c and 11, I_{Gmin} = 53 and I_{Gmax} = 221. The threshold level of 20 µm was adequate as no black pixels appeared in the area of the image corresponding to the blood vessel and the noise in the background almost disappeared.

3.4 Stress Measurement

After applying the analysis to N_2 we obtained N'_2 which have the 98.2% of the pixels below 32kPa, Fig.10.d. The results for all the analyzed images are summarized in Table 1 and shown in figures 11, 12. The estimated flow pressure variation during the registration of $\boldsymbol{F}$ is shown in figure 9.

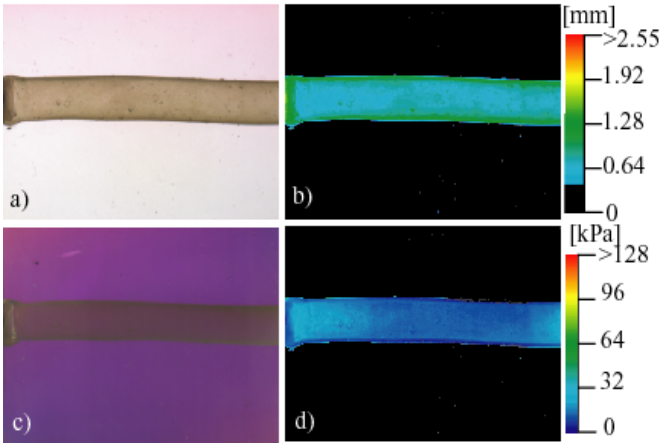

Fig. 8: Images used and obtained during the calibration process a) Image N_0, used to calculate the optical path length. b) N_1 Optical path length quantification. c) Image N_2 used to find I_{Gmin} d) N'_2 Stress quantification of N_2.

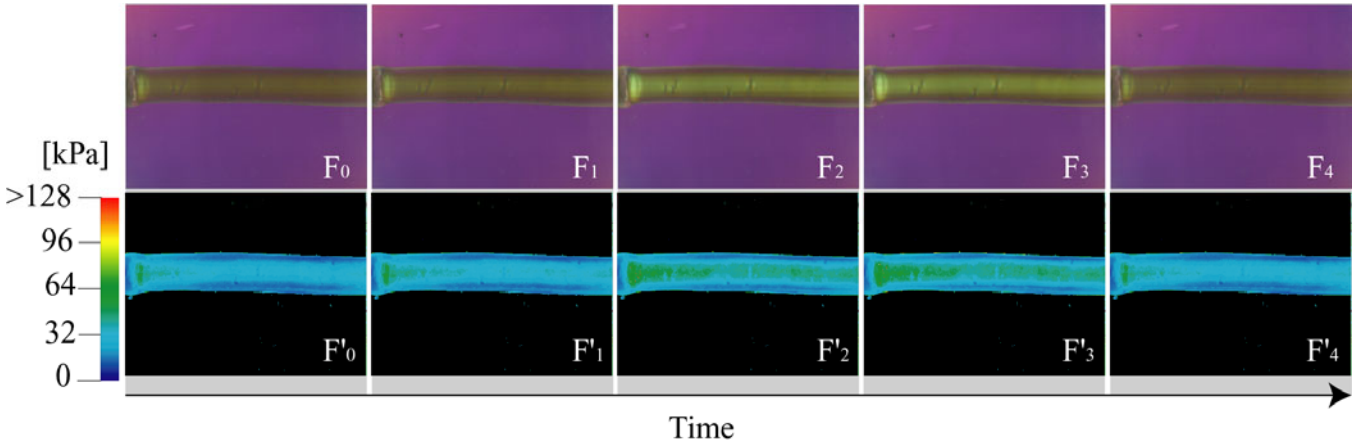

Fig.9: ***F*** image collection and their respective stress quantification ***F'***. N_3=F_3 is the image used to find I_{Gmax} during the calibration process.

4. DISCUSSION

Human blood pressure simulation and shielding of urethane in the model of vasculature enabled the analysis of the principal component of stress in the wall of vasculature for pressure variations. A calibration method was proposed using images of the vasculature at normal stress conditions and enabled the numerical comparison of stress distribution as stated on Table 1 and figures 10-12.

Normal stress parameters may be defined by the values of Table 1: the values of F'_0, as normal low parameters and the values of F'_3 as normal high parameters. As expected the values of F'_1 and F'_2 belong to the range defined by F'_0 F'_3 and the values of N'_2 are below. N'_4 and N'_5 presented values slightly above the range F'_0 F'_3 for the stress ranges R_2 and R_3 and values that may be considered normal high for other parameters.

We have to consider that we used a fixed image to calculate the value of the optical path length in every pixel. As we can see image N_5 presents a considerable deformation of the blood vessel model and high birefringence. In N'_5 the deformation is not visible and a low stress region is introduced in the place where blood vessel model is not present, and a percentage of the high stress zone was blacked out. For that reason values of N'_5 are that close to the normal high values.

This problem may be solved by calculating the optical path length for every image. For the implementation of a real time stress analysis this may be achieved using a prismatic lens that allows the use a camera with polarizer and another without at the same time.

The final goal of this research is to build a real time evaluation system for medical tools and human skills. A complementary stress measurement method is the use of pressure sensors inside the catheter [15]. But introducing foreign objects the catheter increases the stiffness of the catheter; therefore the number of possible evaluations with pressure sensors is limited. The proposed methodology gives a new option for numerical comparison with a wide range of applications, but still has some limitations. Future research is needed to quantify and reduce the error of the system, and optimize optical path length calculation by comparing the optical measurements with a micro tomogram of the vessel model. Image processing speed is also an important challenge to solve, as it takes a few seconds to process an image.

5. CONCLUSION

Pressure levels were useful to calibrate the stress analyzing software; stress produced by pressure variation inside urethane models of vasculature was compared numerically to the stress produced with a guide wire. This kind of evaluation may be applied for safety of catheter insertion robots, such as [16, 17] and compare the performance of medical tools and human skills. To achieve stress quantification in real time, calculation time and error of the system must be minimized.

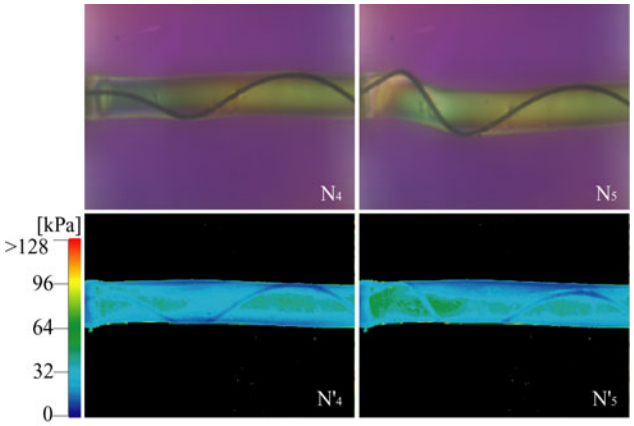

Fig. 10: Quantification of stress produced by a guide wire of catheter and pressure on the membrane of the model of vasculature obtained from N_4 and N_5.

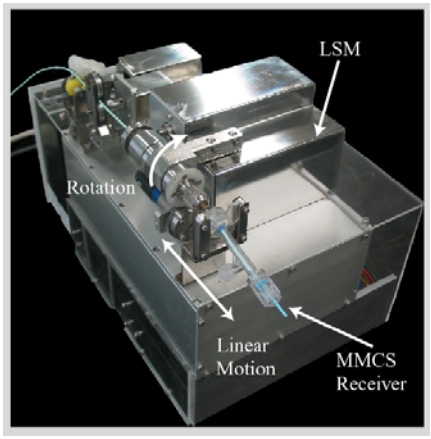

Fig. 11: Autonomous Catheter Insertion System, reproduces catheter insertion trajectories, [16, 17]

REFERENCES

[1] C. Murray, A. Lopez, "Alternative projections of mortality and disability by cause 1990–2020: Global Burden of Disease Study" *The Lancet*, Vol. 349, pp. 1498-1504, 1997.

[2] K. Kunkler, "The role of Medical simulation: an overview," International Journal of Medical Robotics and Computer Assisted Surgery, vol.2, pp.203-210, 2006.

[3] Y. Kawanabe, A. Sadato, W. Taki, N. Hashimoto. "Endovascular Occlusion of Intracranial Aneurysms with Guglielmi Detachable Coils: Correlation Between Coil Packing Density and Coil Compaction," Acta Neurochir Vol.143, pp.451-455, 2001.

[4] S. Ikeda, C. Tercero, T. Fukuda, Y. Okada, F. Arai, M. Negoro, M. Hayakawa, I. Takahashi. "Patient-Specific IVR Endovascular Simulator with Augmented Reality for Medical Training and Robot Evaluation," Journal of Robotics and Mechatronics. Vol.20, No.3, pp. 441-448, 2008.

[5] P. Serruys, P. de Jaegere, F. Kiemeneij, C. Macaya, W. Rutsch, G. Heyndrickx, H. Emanuelsson, J. Marco, V. Legrand, P. Materne, J. Belardi, U. Sigwart, A. Colombo, J. Goy, P. van den Heuvel, J. Delcan, M. Morel, "A Comparison of Balloon-Expandable-Stent Implantation with Balloon Angioplasty in Patients with Coronary Artery Disease," The New England Journal of Medicine, Vol. 331, No.8, pp. 489-495, 1994.

[6] S. Ikeda, F. Arai, T. Fukuda, M. Negoro, K. Irie, "An in vitro patientspecific biological model of the cerebral artery reproduced with a membranous configuration for simulating endovascular intervention," J Robotics and Mechatronics, vol. 17, no. 3, pp. 327–333, 2005.

[7] S. Ikeda, T. Fukuda, F. Arai, et al., "Patient-specific neurovascular simulator for evaluating the performance of medical robots and instruments," in Proc. of the IEEE-ICRA, 2006, pp. 625-630.

[8] C. Tercero, Y. Okada, S. Ikeda, T. Fukuda, K. Sekiyama, M. Negoro, I. Takahashi. "Numerical evaluation method for catheter prototypes using photo-elastic stress analysis on patient-specific vascular model," International Journal of Medical Robotics and Computer Assisted Surgery, Vol.3:4 pp. 349-354, 2007.

[9] J. Panza, "High-Normal Blood Pressure more "High" than "Normal"," N Engl J Med, vol. 345, no. 18, pp.1337-1340, 2001.

[10] B. De Bruyne, J. Bartunek, S.K. Sys, et al., "Simultaneous coronary pressure and flow velocity measurements in humans," Circulation, vol. 94, pp.1842-1849, 1996.

[11] A. J. Ebenal, S. Vasana, C. Clinton, D. Cox, and T. Shine, "Arterial Blood Pressure System Modeling and Signal Analysis" in Proc. IEEE-CIRA, 2007, pp.386-391

[12] S. Tong, D. Yang, "Rotor Profiles Synthesis for Lobe Pumps With Given Flow Rate Functions," Journal of Mechanical Design, Vol. 127, pp.287-294, 2005.

[13] A. Kuske G. Robertson, "Photoelastic Stress Analysis", A Wiley-Interscience Publication, (1974), pp. 87-109, 263-274

[14] Y. Okada, S. Ikeda, T. Fukuda, F. Arai, M. Negoro, I. Takahashi, "Photoelastic Stress Analysis on Patient-Specific Anatomical Model of Cerebral Artery", in Proc. of the International Symposium on Micro-NanoMechatronics and Human Science,2007, pp. 538-543.

[15] M. Tanimoto, F. Arai, T. Fukuda, H. Iwata, K. Gotoh, M. Hashimoto and M. Negoro, "Study on Micro Force Sensor for Minimum Invasive Surgery," Trans. of the Japan Soc. of Mech. Eng., C 64-620, JSME, pp150-155, 1998.

[16] C. Tercero, S. Ikeda, T. Fukuda, K. Sekiyama, Y. Okada, T. Uchiyama, M. Negoro, I. Takahashi. "Robot Manipulation and Guidance Using Magnetic Motion Capture Sensor and a Rule-Based Controller," Journal of Robotics and Mechatronics. Vol.20, No.1, pp. 151-158, 2008.

[17] C. Tercero, S. Ikeda, T. Uchiyama, T. Fukuda, F. Arai, Y. Okada, Y. Ono, R. Hattori, T. Yamamoto, M. Negoro, I. Takahashi. "Autonomous Catheter Insertion System using Magnetic Motion Capture Sensor for endovascular surgery," International Journal of Medical Robotics and Computer Assisted Surgery. Vol. 3:1 pp 52-58, 2007.